Electronic Supplementary Material (ESI) for Environmental Science: Nano.

SUPPLEMENTARY INFORMATION

Ag-NPs	Zeta Potential (mV) at pH=7	Acquisition
Ag-SiO_2	-32.4 ($\pm$1.5)	ZetaSizer, Malvern
Ag-PVP	-28.1 ($\pm$2.8)	ZetaSizer, Malvern
Ag-SiO_2-NH_2	12.8	Commercial Data

Table S1: Zeta potential of Ag-SiO_2, Ag-PVP and Ag-SiO_2-NH_2 NPs at pH=7.

Annex 1: Long Period – X-Ray Standing Waves – Fluorescence Yield

In LP-XWS-FY, the angle of the sample with respect to the incident x-ray beam is scanned in the vicinity of the critical angle for total external reflection of the substrate. X-ray reflectivity data and fluorescence spectra are collected simultaneously. Element partitioning at the solution/biofilm/mineral interface is probed by measuring the fluorescence yield (FY) at the emission energy of a specific element throughout the scan. At angles at or below the critical angle for total external reflection the interference of the incident and reflected x-ray beams creates an electric field intensity standing wave pattern above the surface. The first antinode of this standing wave is located on the alumina surface at the critical angle for total external reflection and moves above the surface (e.g. into the biofilm compartment) as the angle of incidence is reduced. As this antinode sweeps through a region with an element of interest it will cause that element to fluoresce allowing us to model the fluorescence yield data and determine this element's location and concentration relative to the surface. As the incident angle varies from the critical angle to zero the distance between the antinodes increases and the first antinode moves away from the surface and into the film above. This means at small angle most of the antinodes are localized in the biofilm compartment and just at the critical angle there is an antinode located at the substrate surface stimulating fluorescence of atoms in contact with or in close (within 50 nm) proximity to the reflecting surface. This relationship between the standing wave pattern and incidence angle allows the fluorescence yield at the emission energy of a specific element to be measured at different heights relative to the surface, allowing the partitioning at the solution/biofilm/crystal interface to be probed. This technic does not allow to access to the element speciation.

Two compartments can be defined (depending of where most of the antinodes are located), the biofilm and the mineral surface [1]. To discriminate precisely between these two compartments, the samples were studied at 13.8keV (an energy above the Se k-edge and Pb L-edge) to obtain LP-XSW-FY for free Se (VI) and Pb (II) which have well understood biofilm and mineral surface specificities. Pb is present in the medium growth at trace concentration. At low concentration, Pb is known to interact preferentially with the mineral surface[2] while Se is essential to living organisms since it is an oligo-element. The Se FY peak is located between 0.05° and 0.15°, whereas the Pb FY peak is at 0.17° (the critical angle at 13.8 keV) (data not shown), validating our ability to determine elemental partitioning in our system.

To analyze LP-XSW-FY data three major steps were performed. In the first, the X-Ray fluorescence intensities of several elements were extracted. Each peak of a full fluorescence spectrum was assigned to the relevant element, and fit to a background-subtracted Gaussian line shape with an

energy dependent width (figure S1). The integrated counts in the peak (after deadtime correction) are proportional to the number of fluorescing atoms. In the second step, X-ray reflectivity was fitted using the matrix method, needed to model multilayer structures [3, 4]. The model was constrained by parameters such as refractive indices (http://henke.lbl.gov/optical_constants/getdb2.html), interface position and interfacial roughness. The parameters obtained by minimizing the errors between data and reflectivity model allowed us to calculate the electric field intensity profile over the depth of the entire multilayer with a spatial resolution of 1nm. The third step of LP-XSW-FY analysis is to calculate the fluorescence yield curve for the element of interest. To do so, the electric field was reconstructed at every point of the biofilm/crystal interface with 1nm depth resolution. Using this information, the fluorescence intensity (If) as a function of depth (z) is determined using, $If(z) = \alpha_i C_i \left\| E^{(i)}(z) \right\|$, where α_i is a correction factor, C_i the mass concentration, and $E^{(i)}(z)$ is the electric field at any layer *i* as a function of z [5]. This fluorescence model allows us to obtain an elemental concentration profile as a function of depth. Because of the finite thickness of the film the fluorescence signal as a function of z is corrected for self-absorption via the α_i parameter. The fluorescence intensity measured by the detector was normalized to that of Al at the critical angle of the α-Al_2O_3(1-102) substrate crystal which is assumed to be constant for all substrates.

Proper interpretation of LP-XSW-FY data is highly dependent on crystal alignment. Prior to measurement, each substrate was aligned to the x-ray beam and the quality of this alignment was verified by reflectivity measurement and comparison of the theoretical and measured critical angles. At an incident X-ray energy of 7keV the average measured critical angle of $0.314 \pm 0.017°$ agreed well with the theoretical value of 0.320° for Al_2O_3.

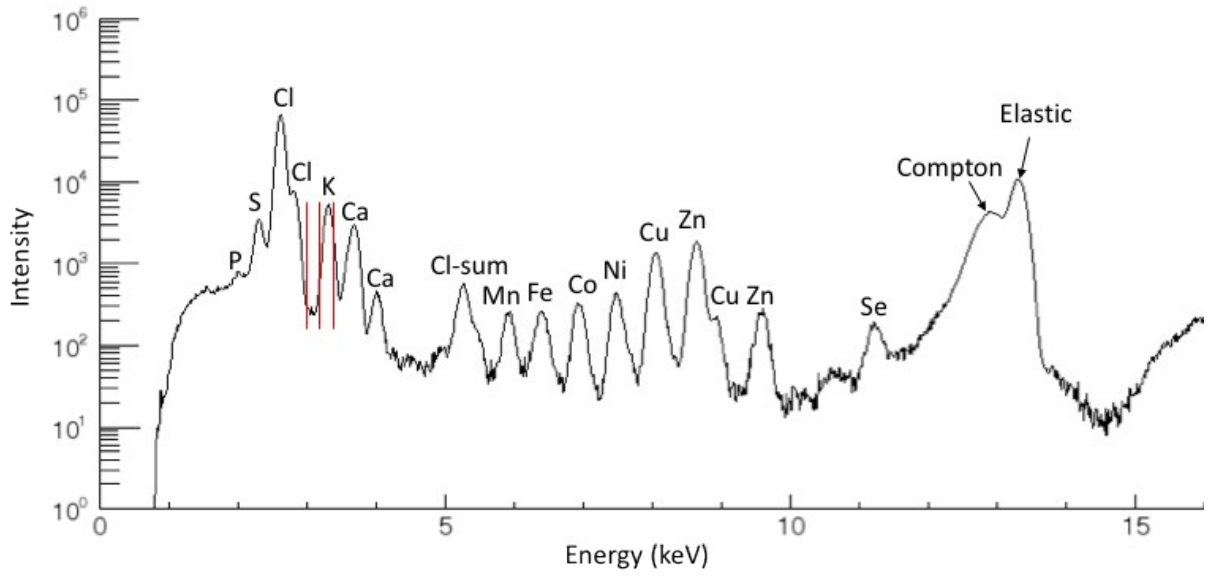

Figure S1: Fluorescence intensity as a function of energy for a *Shewanella oneidensis* MR-1 biofilm (incident angle = 0.09°) unexposed to AgNPs. Each peak corresponds to an emission line of an element present in the sample. Red lines show positions of Ag Lα1, Lβ1, Lβ2 from left to right, where peaks would be observed if Ag were present in the sample.

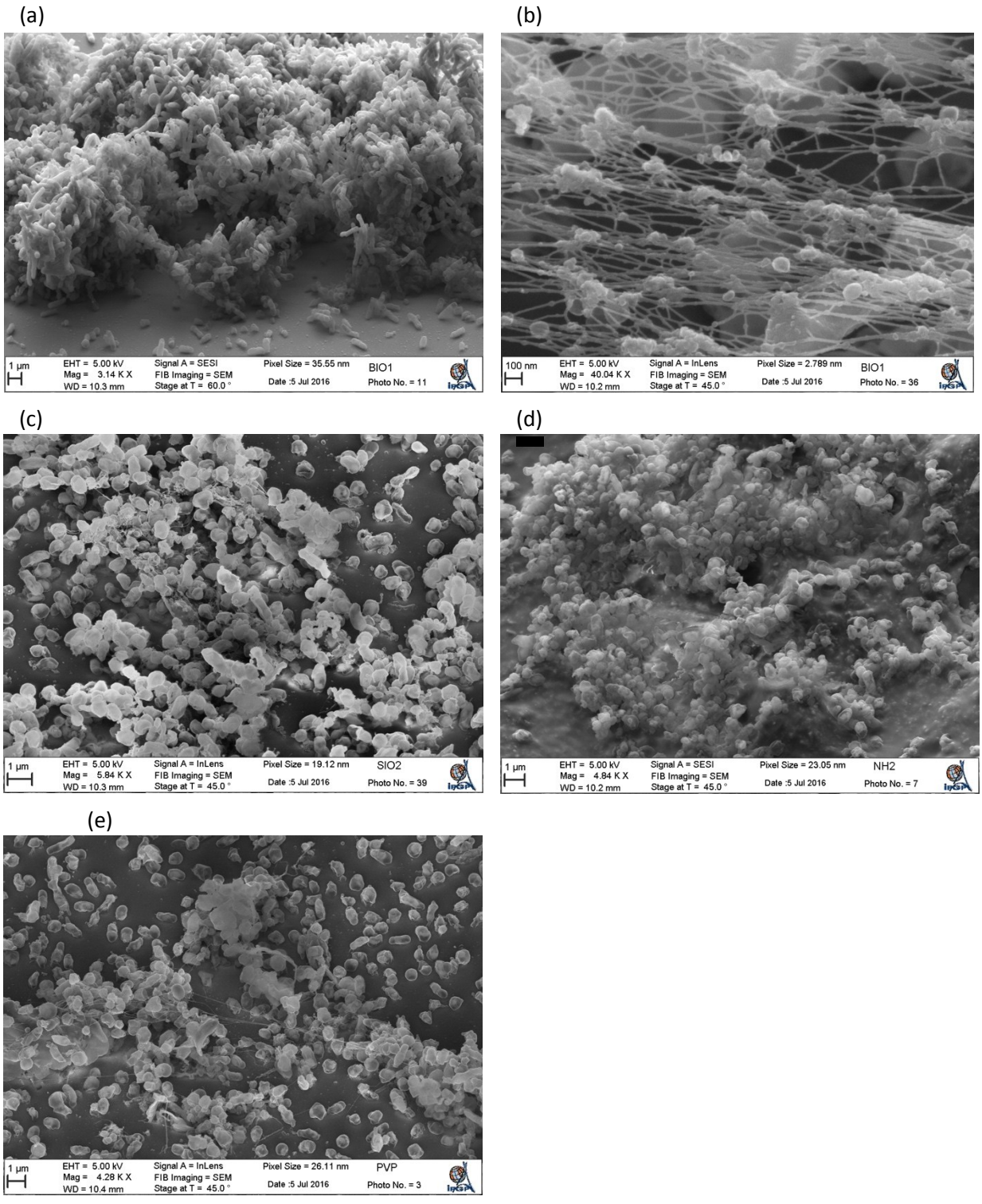

Figure S2.1: Scanning electron microscopy (SEM) images of *Shewanella oneidensis* MR-1 biofilms grown on α-Al_2O_3(1-102) substrates for 10 days (a) and a zoom of the same biofilm showing an EPS matrix (b), and then exposed to Ag-SiO_2 (c), Ag-SiO_2-NH_2 (d) and Ag-PVP (e) NPs for 24 hours. Biofilm is denser and more resistant to supercritical drying when it isn't exposed to AgNPs.

(a)

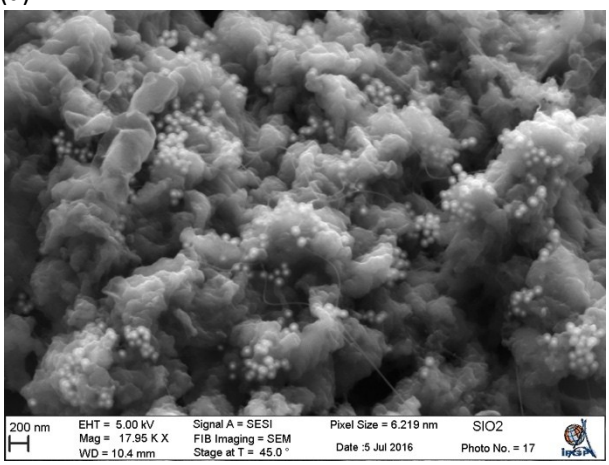

(b)

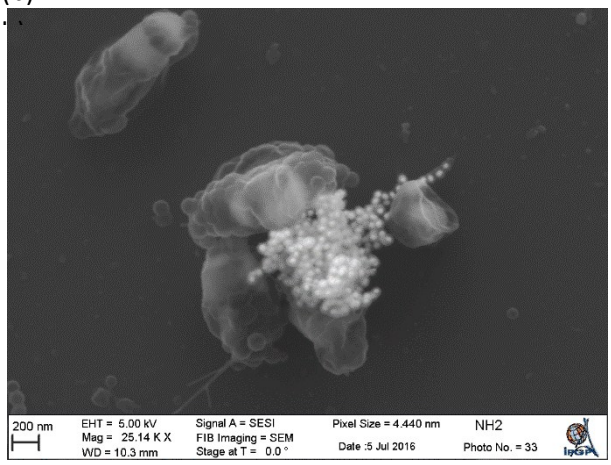

(c)

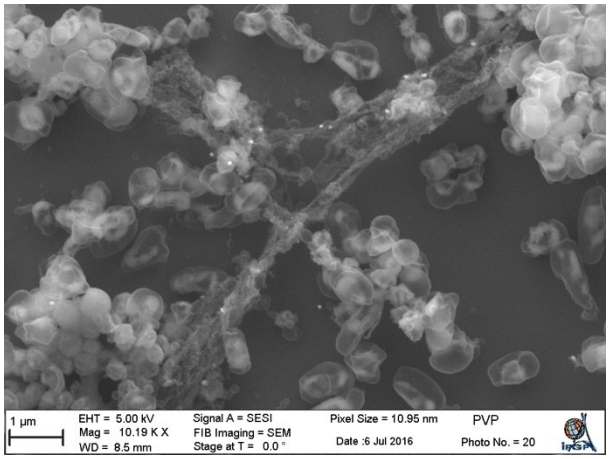

Figure S2.2: Scanning electron microscopy (SEM) images of *Shewanella oneidensis* MR-1 biofilms grown on α-Al_2O_3(1-102) substrates for 10 days and exposed to Ag-SiO_2 (a), Ag-SiO_2-NH_2 (b) and Ag-PVP (c) NPs for 24 hours. Core/shell structures are observable for Ag-SiO_2 and Ag-SiO_2-NH_2 in images (a) and (b). Chains of Ag-SiO_2-NH_2 (b) NPs are observable. Ag-PVP is well-dispersed (c).

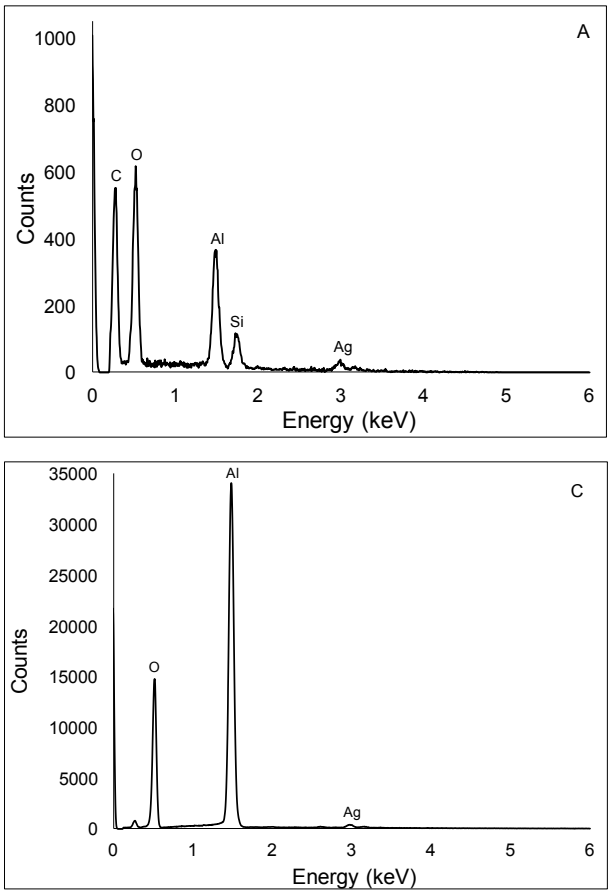

Figure S3: Qualitative chemical composition of particles (EDX spectrum) present on solution/biofilm/crystal system exposed to Ag-SiO_2 (A), Ag-SiO_2-NH_2 (B) and Ag-PVP (C) for 24 hours, and the relative mass percentage of each element detected.

	wt% Ag	wt% Si
Ag-SiO2	24.2	13.6
Ag-SiO2-NH2	57	5.9
Ag-PVP	2.7	

Sample	Exposure time	Film thickness (μm)	Calculated uncertainty (μm)	NPs size (nm)	NPs charge at pH 7
Ag-PVP	3h	5.6	0.5	60	Negative
	24h	5.5	0.6		
Ag-SiO2	3h	4.5	0.7	90	Negative
	24h	5.1	0.7		
Ag-SiO2-NH2	3h	6.5	0.3	90	Positive
	24h	3.5	0.9		

Table S2: Summary of sample and film thickness obtained by modeling reflectivity. Film thickness correspond to the average thickness of exposed biofilm. Uncertainty calculations are described in Annex 2.

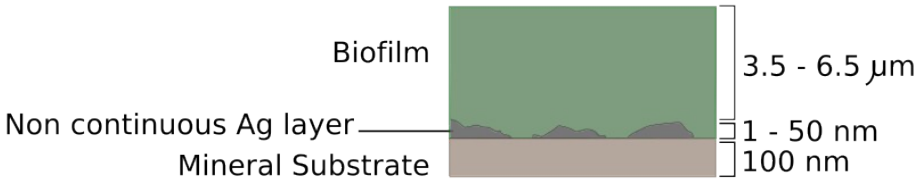

Figure S4: Diagram of the modelled interface. Modelled biofilms have an average thickness of 5.1 μm (3.5μm to 6.5μm), thickness of mineral substrate is fixed at 100nm and the non-continuous Ag layer measured between 1 and 50 nm (depending on sample).

Annex 2: Uncertainty on average thickness of biofilm obtained by modeling reflectivity data

Uncertainty on film thickness reported by the fits is quite small (nm scale). Nevertheless, there are additional uncertainties that are not accounted for by the correlation matrix.

In order to estimate the range of error given by the overall fitting procedure on the biofilm thickness we used the following method. At first the model sensitivity was tested for each experimental condition, and for incident angles ranging between 0.07° and 0.32°, which represents the region that contains most of the information. To do so, a reflectivity curve was generated for 8 different theoretical biofilm thicknesses in the interval [-1μm; +1μm] around the best thickness value reported in S2 table. Then, in order to define the range of thickness values for which the standard deviation is not significantly different from the standard deviation corresponding to the best thickness value, a Student's test was performed (table S2). For all 6 biofilms, this procedure indicates a maximum error of 0.9 μm on the estimated thickness (table S2). Thus, given the heterogeneity of biofilm coverage, a value of ±1.0 μm is reported in our paper as uncertainty for thickness evaluation (results section, page 5, last paragraph).

References

1. A. Templeton and E. Knowles, Microbial Transformations of Minerals and Metals: Recent Advances in Geomicrobiology Derived from Synchrotron-Based X-Ray Spectroscopy and X-Ray Microscopy, *Annual Review of Earth and Planetary Sciences*, 2009, **37**, 367-391.
2. Y. Wang, A. Gélabert, F. M. Michel, Y. Choi, J. Gescher, G. Ona-Nguema, P. J. Eng, J. R. Bargar, F. Farges, A. M. Spormann and G. E. Brown, Effect of biofilm coatings at metal-oxide/water interfaces I: Pb(II) and Zn(II) partitioning and speciation at Shewanella oneidensis/metal-oxide/water interfaces, *Geochimica et Cosmochimica Acta*, 2016, **188**, 368-392.
3. L. G. Parratt, Surface Studies of Solids by Total Reflection of X-Rays, *Physical Review*, 1954, **95**, 359-369.
4. P. Lee, X-ray diffraction in multilayers, *Optics Communications*, 1981, **37**, 159-164.
5. D. K. G. de Boer, Glancing-incidence x-ray fluorescence of layered materials, *Physical Review B*, 1991, **44**, 498-511.